Evaluation of Guiding Device for Downstream Fish Migration with in-Field Particle Tracking Velocimetry and CFD

T. S. Lundström[†], M. Brynjell-Rahkola, A-L Ljung, J. G. I. Hellström, T. M. Green

Division of Fluid and Experimental Mechanics, Luleå University of Technology, SE-971 87 Luleå, Sweden

†*Corresponding Author Email: staffan.lundstrom@ltu.se*

ABSTRACT

The performance of a fish guiding device located just upstream a hydropower plant is scrutinized. The device is designed to redirect surface orientated down-stream migrating fish (smolts) away from the turbines towards a spillway that act as a relatively safe fishway. Particles are added up-stream the device and the fraction particles going to the spillway is measured. A two-frame Particle Tracking Velocimetry algorithm is used to derive the velocity field of the water. The experimental results are compared to simulations with CFD. If the smolts move passively as the particles used in the study the guiding device works very well and some modifications may optimize its performance. In-field Particle Tracking Velocimetry is a suitable technique for the current case and the results compare well with numerical simulations.

Keywords: River; Fish migration; Smolt; Fish guiding device; Hydropower; PTV; CFD.

1. INTRODUCTION

Flowing water is a renewable source of energy and various techniques can be used to covert potential and kinetic energy to electricity (Marjavaara and Lundström 2006; Marjavaara, Lundström *et al.* 2007; Grabbe, Yuen *et al*. 2009; Lalander, Leijon 2011; Vashisht 2012; Pompeu, Agostinho *et al.* 2012). Dependent on the method used the efficiency and the environmental impact varies (Price, Probert 1997; Tarkowski, Uliasz-Misiak 2003; Kusre, Baruah *et al.* 2010; Abbasi, Abbasi 2000). Often a dam is built in the river so that nearly all of the potential energy of the water can be transformed into electricity and that enable an efficient regulation of the river. A main drawback with a dam is that fauna passage (notably fish) is delayed or hindered. Well-functioning fishways may however increase the hydrologic connectivity and simplify the passage of a number of species (Renöfält, Jansson *et al.* 2010). In the current study attention is paid to downstream migrating smolt in the river Piteälven in the north of Sweden. The river has one power station, Sikfors, see Fig. 1 showing part of the dam, a spillway (bottom left) and a smolt guiding device. Most water goes to the turbines that are located underground and to the right of the picture and the spillways are used when the volumetric flow rate in the river is larger than the turbines can handle. In Sikfors the spillways are also used as a fishway during periods of down-stream migrating fish, mainly smolt. The purpose with the guiding device is therefore to direct the smolts to the spillways and thus increase the number of smolts using this path instead of going through the turbines.

A poorly designed fishway or guiding device may result in that fish are prevented from migrating and hence delayed downstream or upstream the dam where they become prey for predators. They may also be badly injured/killed when passing through the turbines (Schilt 2007). For fish passing a Kaplan turbine the mortality can be as high as 81-92% (Ferguson 2005) while the mortality for fish moving through a surface spillway can be as low as 0-2%, (Whitney, Calvin *et al.* 1997).

Migrating fish in rivers are sensitive to both the velocity magnitude and the velocity gradient of the flow. Fish migration can thus be improved by adjusting the flow near obstacles such as dams and rapids. To exemplify, it is well established that up-stream migrating fish may be steered to a fish-way leading around a dam with the use of attraction water (Laine, Kamula *et al.* 1998; Laine, Ylinäaräa *et al.* 1998; Rowland, Hotchkiss *et al.* 2003; Lindmark, Gustavsson 2008; Rice, Lancaster *et al*. 2010; Green, Lindmark *et al.* 2011). Methods have also been developed that can safely guide downstream migrating fish like smolt around the turbines (Lundström, Hellström *et al.* 2010). Smolts usually migrate in fresh water by following the main stream using as little energy as possible

(Moore, Ives *et al.* 1998, Russell, Moore *et al.* 1998). They tend to keep to the water surface and avoid strong accelerations or retardations, (Haro, Odeh *et al.* 1998; Johnson, Adams *et al.* 2000). To exemplify, Pacific salmon smolt that encounter two different accelerations, 0.3 m/s^2 and 1.2 m/s^2 hesitate for longer time before passing through the higher acceleration (Kemp, Gessel *et al.* 2006). In a similar manner when smolt (Chinook, Steelhead, Coho and Sockeye) encountered a free or constricted passage (acceleration in the constricted passage 1.3 m/s^2 and 1.8 m/s^2) most smolts chose the free passage (Kemp, Gessel *et al.* 2005). With this in mind there are several passive and active ways to guide the smolt to take a certain route such as bar racks, barrier nets, screens, louver systems, fish pumps, sound and light (Taft 2000).

Fig. 1. View of part of a dam, a spillway (bottom left) and a smolt guiding device that stretches over the water. Most water goes to the turbines that are located underground and to the right of the picture.

A new method to guide smolt from the turbines in Sikfors was suggested and numerically evaluated in (Lundström, Hellström *et al.* 2010). A 2.0 m deep impermeable device is placed in the river up-stream the dam directing some of the surface water towards the spillways. The concept, which is based on smolts tendency to swim close to the water surface, has been evaluated for permeable devices such as louvers in several rivers (Ruggles, Ryan 1964; Ruggles, Robinson *et al.* 1993; Scruton, Ollerhead *et al.* 2003). The method in (Lundström, Hellström *et al.* 2010) was with some modifications realized into 33, 5 m long and slightly over 2.0 m high wooden wall segments being connected via a steel wire at their lower ends, approximately 1.8 m below the water surface. The wire is anchored to the shore in one end and to the concrete dam in the other, see Fig. 1. The function of the guiding device is here evaluated with the use of Large scale Particle Tracking Velocimetry (PTV) (Fujita, Muste *et al.* 1998; Meselhe, Peeva *et al.* 2004; Fujita, Muste 2011) and Computational Fluid Dynamics (CFD). For energy efficiency reasons it is of interest that the smolt are guided towards the spillways with as little flow as possible. Hence, the concept is studied for two flow rates over the spillways.

2. IN-FIELD EXPERIMENTS

The experiments were carried out at the Sikfors

hydro power plant during June 2011 where the flow over the spillway was 50 m^3/s (Session 1) and during August 2011 with a spill of 16 m^3/s (Session 2), see Fig. 1.The station has a head that varies between 19.1 m and 21.0 m and an annual mean flow of 158 m^3/s. The power plant is equipped with two Kaplan turbines, 20 MW each. In each session three series of measurements were carried out. For Session 1 the flow rate through the turbines was 237 m^3/s during series 1 and 250 m^3/s during series 2 and 3. For Session 2, the flow rate was 225 m^3/s for all series.
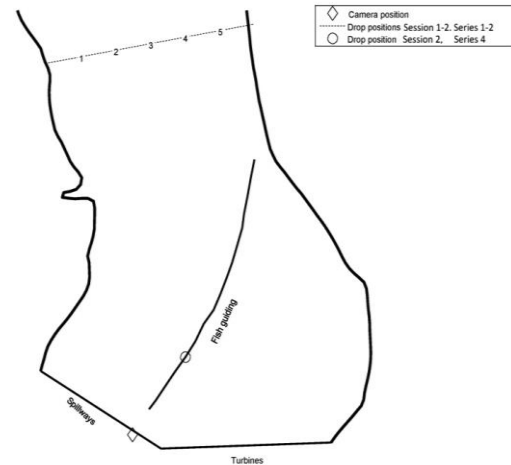

Fig. 2. Top view of the river up-stream the dam defining drop positions and camera position.

The capability of the guiding device to redirect surface water towards the surface spillway was assessed by releasing seeding particles (oranges) from about 220 m upstream of the dam. For Session 1, series 1 and 2 consisted of 5 drops distributed across the width of the river along the dashed line in Fig. 2. Series 1 and 2 are similar and only separated in time and by the number of seeding particles in each drop, 10 and 20 respectively, see Table 1. Series 3 implied 3 drops near the shore at positions close to the upstream end of the guiding device. The aim with this series was to investigate whether particles passing in the gap between the upstream end of the guiding device and the north shore would float towards the turbines or possibly take some other route like following the guiding device on its downstream side.

Table 1 Number of seeding particles used in each drop during the Sessions. The numbers in italic denote flow rate (m^3/s) to the spillway and the turbines, respectively.

	Session 1			Session 2		
Serie/ Drop	1	2	3	1	2	4
	50	*50*	*50*	*16*	*16*	*16*
	237	*250*	*250*	*225*	*225*	*225*
1	10	20	10	40	40	50
2	10	20	10	40	40	50
3	10	20	10	40	40	50
4	10	20		40	40	
5	10	20		40	40	

Session 2 involved more seeding particles, 40-50 in each drop; see Table 1. Series 1 and 2 were similar to those in Session 1 whereas series 4 consisted of 3 drops from the side of the guiding device at a position about 50 m from the dam, see Fig. 2. The aim with series 4 was to provide data enabling vector field plots close to the downstream end of the guiding device. To aid the assessment of distances from photographs of the seeding particles, as well as to insert fixed landmarks for camera calibration, three approximately straight fender lines were placed in the river during the second session.

2.1 Seeding Particles

As discussed in (Adrian 1996) important properties for seeding particles are their ability to convey a high signal-to-noise ratio, an aerodynamic shape which allows them to closely follow the flow, a density similar to the measured fluid and a low price. By taking these aspects into account an initial study yielded that oranges were suitable seeding particles. In addition to fulfilling the criteria stated above and being easily obtained in large volumes, a fair amount of oranges can be discharged into the environment without causing long-term problems since they are biodegradable. Due to the size of the oranges, they cannot be expected to catch the smallest details of the flow. However since this investigation is mainly focused on larger flow structures this is of minor concern. Furthermore, using smaller particles would greatly complicate the process of particle identification, considering the size of the reservoir and the depth covered by the photographs (~170 m). An initial study showed that under such conditions even just slightly smaller seeding particles (satsumas or clementines) were difficult to detect.

2.2 Experimental Equipment

Data for the PTV-analysis were recorded using a remotely controlled D-SLR camera (Nikon D90) with an 18-105 mm normal zoom lens mounted on a tripod. The camera was placed on the concrete dam approximately 5 m above the water surface and pictures were sampled with a frequency of 2 Hz. To measure the GPS-positions of the landmarks used in the camera calibration a handheld outdoor GPS Garmin Dakota 20 was used. The positions were measured in the two-dimensional map projection SWEREF 99 TM and the reported accuracy of the GPS during the measurements varied between 3-12 m. Also, whenever GPS-coordinates of landmarks were not obtainable for safety reasons, the positions were calculated using an analogue compass that measures 400 degrees per revolution and a digital laser rangefinder Bosch PLR 50 with a reported accuracy of about 2 mm.

3. PARTICLE TRACKING VELOCIMETRY

For series 4 in the second Session the number of particles is fairly large in a limited area enabling a deeper analysis of the flow field of the surface water. For this purpose a PTV-algorithm was implemented using the commercial software MATLAB R2011a. The individual steps in this process are more closely described below including processing of images of the particles, calibration of camera to deal with distortions and calculation of the velocity field.
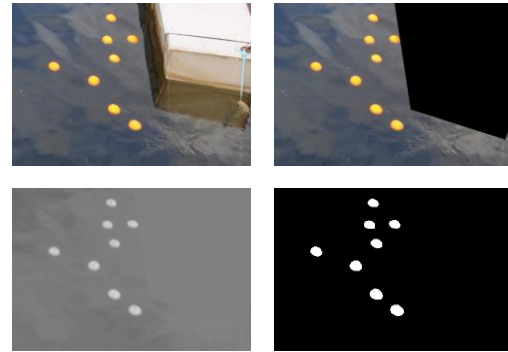

Fig. 3. Filtering steps: Initial sample photo, photo with removed background, pixels intensities in *b**-dimensions and final binary mask.

3.1 Image Processing

The filter applied in the image processing is designed to separate the seeding particles from the images and produce a binary map that can be used as input to the particle identification routine, see Fig. 3. Particles in conventional Particle Image Velocimetry (PIV) and Laser Doppler Velocimetry (LDV) correspond to intensity maxima in the recorded images and analysis is usually done in a grey scale, (Adrian 1996, Goldstein, Kreid 1967). However, to benefit from the high visibility and contrast offered by the chosen seeding particles a filter based on color information was developed. The first step in the filtering algorithm is to remove unwanted objects in the background and surroundings from the image, which is done by subtracting a mask containing these elements from the pictures. The images are then converted from the color space sRGB produced by the camera to CIELAB, which is a three-dimensional color space where the first dimension $L*$ is a measure of lightness and $a*$ and $b*$ correspond to the red-green and yellow-blue color axis, respectively (Fairchild 2005). The yellow-blue color information is then extracted from the image and finally used to generate a binary mask, where pixels exceeding a given threshold are denoted a value of one and the rest a value of 0.0, see Fig. 3. When the picture has been filtered, the binary mask is put into the particle identification routine that traces the regions and utilizes the following statistical criteria on the area of each region to determine the presence of particles

$$a_i < (a_{mean} - a_{std.dev.}) \implies \text{No particle}$$

$$(a_{mean} - a_{std.dev.}) \leq a_i \leq (a_{mean} + a_{std.dev.}) \implies \text{Particle} \qquad (1)$$

$$(a_{mean} + a_{std.dev.}) < a_i \implies \text{Possible particle overlap}$$

In the case of one particle, the determination of its centroid is trivial, but whenever there might be an overlap additional actions are required since there can be several particles overlapping. To determine if and how many particles in a certain region that are subject to overlap, a template reflecting a typical seeding particle in the image scrutinized is generated. The region is then cross-correlated with the particle template by calculating the normalized correlation coefficient at each point according to the following expression

$$\gamma(u,v) = \frac{[f(x,y)-\bar{f}_{u,v}][t(x-u,y-v)-\bar{t}]}{\left\{\sum_{x,y}[f(x,y)-\bar{f}_{u,v}]^2 \sum_{x,y}[t(x-u,y-v)-\bar{t}]^2\right\}^{1/2}} \quad (2)$$

where *f* represents the region, *t* the template and where the bars denote mean values, (*normxcorr2; MATLAB - The Language Of Technical Computing.*). Pixels correlating with the template over a predefined threshold and in addition are located at least one particle radius apart are then assumed to be particle centroids.
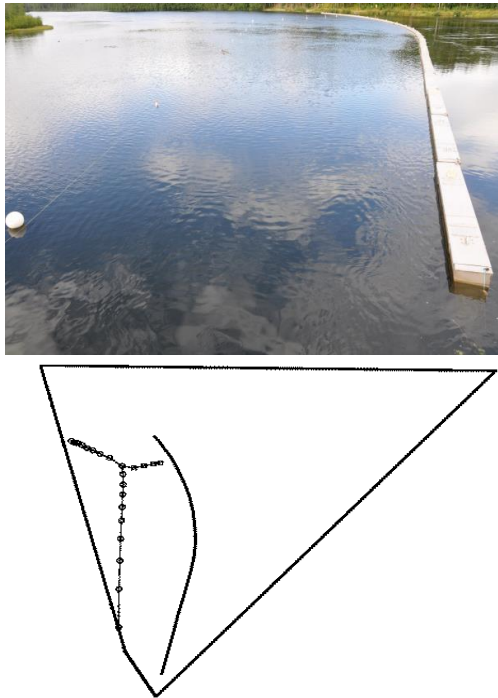

Fig. 4. Sampling view before and after projective transformation.

3.2 Calibration of Camera

When calibrating the camera, two types of distortions in the captured images need to be taken into account. The first distortion in caused by the angle of the recording and the second stems from the lenses of the camera. A method dealing with the first kind of distortion is the projective transformation, which involves rectification of the image distortion through solution of a linear equation system (as described below). The success of this method in the area of Large Scale-PIV (LS-

PIV) has been demonstrated (Fujita, Muste *et al*. 1998; Jodeau, Hauet *et al*. 2008), and the strength is easy implementation and fast computation. However, lens distortions are not taken into account, which requires further actions (see for instance, (Devernay, Faugeras 2001)). In the present study the distortion caused by the optics is estimated by taking photographs of a perfect grid with known cell size using the shortest focal length of the lens. From examining the grid distortions, the distortion caused by the lens was assumed to be negligible compared with the accuracy of the GPS and hence the uncertainty in the position of the landmarks. Therefore, only projective transformation, as suggested by (Fujita, Muste *et al*. 1998) was considered during the coordinate transformations.

The algorithm for the projective transformation basically ties the geographical coordinates to the image coordinates viewed in the photographs. This is achieved by having a set of objects with known geographical coordinates that are visible in the photographs and consequently has easily detectable image coordinates. From the two sets of coordinates, a projective transformation can be done from the following relationships:

$$X_1 = \frac{c_1 x_1 + c_2 x_2 + c_3}{c_4 x_1 + c_5 x_2 + 1} \quad (3)$$

$$X_2 = \frac{c_6 x_1 + c_7 x_2 + c_8}{c_4 x_1 + c_5 x_2 + 1} \quad (4)$$

Here, X_i are geographical coordinates and x_i are image coordinates. Also, index 1 and 2 in the geographical coordinates corresponds to Northing- and Easting coordinates in the SWEREF99TM system (*Two-dimensional systems - SWEREF 99, projections.* 2010) and x- and y-coordinates in the image coordinate system. From Eq. (3) and Eq. (4), the transformation matrix A is set up as follows (where *n* is the number of landmarks):

$$\mathbf{A} = \begin{bmatrix} x_{1,1} & x_{1,2} & 1 & -x_{1,1}X_{1,1} & -x_{1,2}X_{1,1} & 0 & 0 & 0 \\ \vdots & \vdots & \vdots & \vdots & \vdots & \vdots & \vdots & \vdots \\ x_{n,1} & x_{n,2} & 1 & -x_{n,1}X_{n,1} & -x_{n,2}X_{n,1} & 0 & 0 & 0 \\ 0 & 0 & 0 & -x_{1,1}X_{1,2} & -x_{1,2}X_{1,2} & x_{1,1} & x_{1,2} & 1 \\ \vdots & \vdots & \vdots & \vdots & \vdots & \vdots & \vdots & \vdots \\ 0 & 0 & 0 & -x_{n,1}X_{n,2} & -x_{n,2}X_{n,2} & x_{n,1} & x_{n,2} & 1 \end{bmatrix} \quad (5)$$

Using the transformation matrix in Eq. (5), the following system of linear equations is solved:

$$\mathbf{Ac} = \mathbf{Z} \quad (6)$$

where c and Z are given by the relationships below

$$\mathbf{c} = \begin{bmatrix} c_1 & c_2 & c_3 & c_4 & c_5 & c_6 & c_7 & c_8 \end{bmatrix}^T \quad (7)$$

$$\mathbf{Z} = \begin{bmatrix} X_{1,1} & \ldots & X_{n,1} & X_{1,2} & \ldots & X_{n,2} \end{bmatrix}^T \quad (8)$$

Since there are 8 unknown coefficients c_i, a minimum of 4 landmarks are required for the transformation. In addition, for the method to be successful these landmarks must be rather evenly distributed over the images captured and hence span the whole covered area. For some cases more than 4

landmarks are used. The system then becomes over-determined and the solution is derived using a least square method. In the current case as many as 11 landmarks were used. The reason for choosing such a large number was to account of the uncertainty related to the landmark coordinates. It is hence assumed that increasing the number of landmarks will diminish the weight of the individual landmarks on the least square solution and even out possible errors. The projective transformation defined by Eq. (3) and Eq. (4) applied on the sampling view shown in Fig. 4.

3.3 Displacement and Velocities

A two-frame algorithm developed by (Baek, Lee 1996) was used as a particle tracking algorithm. The chosen algorithm has been reported to perform better than a four-frame algorithm suggested by (Hassan, Canaan 1991), regarding both percentage of recovered velocity vectors and computational speed; see (Baek, Lee 1996). The algorithm is basically founded on the following assumptions regarding the seeding particles.

1. Given a known maximum velocity of the particles in the image (U_m) and the time interval between two subsequent frames (Δt) the search area for the particle in the next frame is narrowed down to a circle of radius $T_m = U_m \Delta t$.

2. Inertial forces of the particles, vorticity, accelerations, etc, will only result in small changes to the velocity between two frames.

3. Particles sufficiently close to each other, being within a radius of T_n, are assumed to move in the same direction as a group.

4. Particles move in the same plane and therefore several points from one frame cannot map to the same point in the next (this assumption is in this case subject to doubts due to the acute photographic angle).

Briefly the tracking may be described in the following manner. The centre of a particle is defined in the first frame. An area in the second frame is then covered by a circle with radius T_m and with its centre in the same position as in the first image. Any particles detected within this circle are marked as displacement candidates. In the case of either one or zero matches, the particle displacement is trivial and the code continues with the next particle in the first frame. However, when there are two or more matches in the second frame, the search continues on the first frame for neighboring particles within a distance of T_n (see Fig. 5a). To determine which match is correct, the vector between the particle and each match in the second frame is derived. Then, following the assumption of common motion, the different vectors are in their turn imposed upon the particle and each neighbor in the first frame, see Figs 5b-d. According to the assumption of small velocity change, there can only be minor variations in particle displacement. Hence, a third smaller circle with radius T_q is drawn around each endpoint of the imposed neighbour displacement and matches

found inside each such circle are used to compute the probability of the given displacement vector, compare the results in Figs 5b-d. Through iteration the most probable displacements are found and upon convergence (5b), the code moves on to investigate the displacement of the next particle.
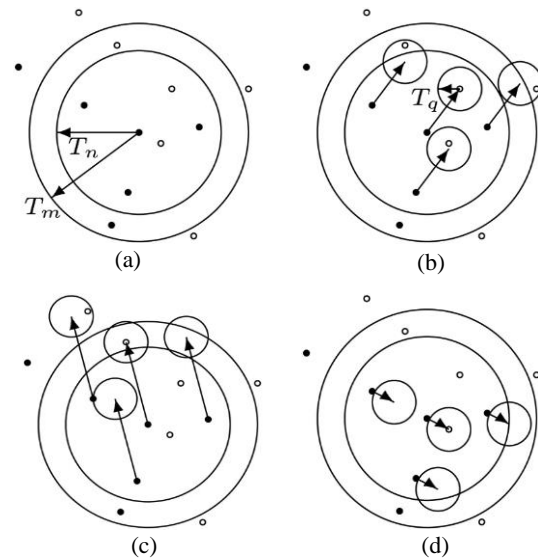

Fig. 5. Illustration of the PTV-algorithm. The filled circles denote particles in the first frame and the open circles denote particles in the second frame.

4. NUMERICS

A virtual model of the river up-stream Sikfors hydropower plant was previously built from measurements with a digital echo-sounder and differential GPS; see (Lundström, Hellström *et al.* 2010). In this work, the position of the guiding device was set via GPS coordinates and a spline was fitted to these discrete points. In reality, the guiding device is built from a number of segments with tiny gaps in-between them. The spline is, however, considered a reasonable assumption since the curvature of the guiding device is relatively small. Including the gaps in the numerical model requires a very fine mesh in this area and can be done in future studies. The power plant has three spillways, but only spillway B was open during the experiments and spillways C-D are therefore regarded as walls in the virtual model, see Fig. 6. The outlet of spillway B is furthermore elongated to avoid numerical errors associated with recirculations. The final geometry is presented in Fig. 6.

In the study, the water surface is represented with a zero-shear slip lid. The rigid-lid approach is acceptable when the elevations of the surface are smaller than 10 % of the channel depth (Rodriguez, Bombardelli *et al.* 2004; Lundström, Hellström *et al.* 2010). Inlet and outlet boundary conditions are designed to represent the experimental conditions. A specified mass flow is set in the river inlet and

spillway outlet, whilst the flow through the turbines is modelled with a zero pressure outlet boundary condition. The walls of the guiding device and dam are considered smooth and a smooth wall is also used for the river bed. The roughness will vary along the bottom of the reservoir and may influence the flow (Andersson, Hellström *et al.* 2014), but since the reservoir is old (~100 years) it is likely that the bottom surface is fairly smooth. The flow is regarded as fully turbulent and modelled with the k-ε turbulence model.
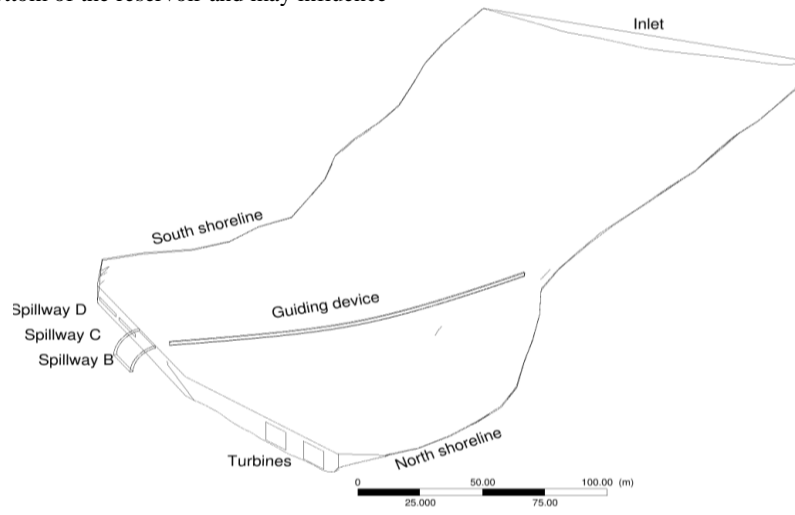

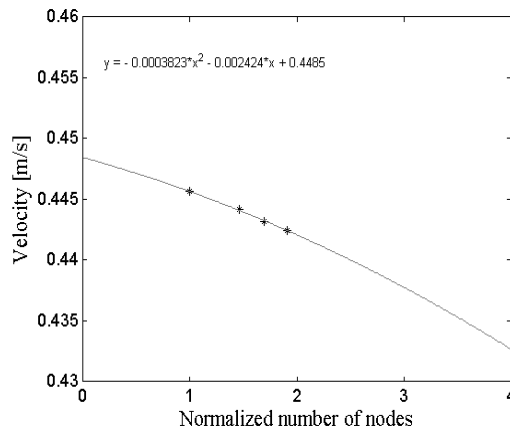**Fig. 6. River geometry with labelled boundaries.**

Fig. 7. A polynomial fitting of maximum surface velocity as function of normalized number of nodes shows an extrapolated value of the velocity of 0.4485.

The simulations are conducted with the commercial Computation Fluid Dynamic (CFD) software ANSYS CFX 14.0, see (Larsson, Lindmark *et al.* 2012; Ljung, Lundström *et al.* 2011; Hellström, Marjavaara *et al.* 2007). The advection scheme is solved with a specified blend factor of 1 while the discretised turbulence equations are solved with a high-resolution scheme. The iterative convergence for the simulations follows industrial recommendations (Casey, Wintergerste 2000; Wintergerste; Casey *et al.* 2002). To ensure a mesh independent solution a mesh convergence test is carried out with boundary conditions corresponding to Session 2. Maximum surface velocity along a line perpendicular to the flow at approximately 190 m upstream the river is chosen as key variable of the study. An analysis of the result from four meshes, with a number of nodes varying from about $3 \cdot 10^6$ to $10.5 \cdot 10^6$ indicates that the meshes are in the asymptotic range, see Fig. 7, (Roache 1997). An extrapolated value of $v = 0.4485$ m/s is retrieved from the polynomial curve in Fig. 7 and from this assessment it can be concluded that the coarsest grid ($3 \cdot 10^6$ nodes) has a relative error of only 1.5 %. This mesh is therefore used in all further simulations.

5. RESULTS

Regardless of session no particles move towards the turbines when released at positions 1-4 from about 220 m upstream of the dam; see Table 2 and series 1 & 2 in both sessions. The first number in each cell in Table 2 represents the percentage released seeding particles that floated towards the spillway and the second represents the percentage seeding particles that floated towards the turbines. Furthermore, half of the particles released at position 5 (the position closest to the northern shore) during Session 2 go to the turbines while again none of those released at position 5 in the first session takes this route. In many of the drops the particles stray away towards the shore or are captured in a large circulation formed between the guiding device and the southern shore implying that they neither goes to the spillway nor to the turbines. It is apparent, however, that most particles released 220 m upstream the dam (series 1 & 2 both sessions) go to the spillway.

During both sessions the wind conditions varied from calm wind to light breeze. During series 1 in Session 1, the wind resulted in that all particles from drop 1 and 2 in series 1 followed the shoreline towards the dam where they got stuck throughout the measurement. The disturbance from the wind was less during the other series in Sessions 1 and 2.

Table 2 Percentage seeding particles to the spillway and the turbines (spillway/turbines). The figures in italic denote flow rate (m³/s) to the spillway and the turbines, respectively.

	Session 1			Session 2		
Drop	1	2	3	1	2	4
/	*50*	*50*	*50*	*16*	*16*	*16*
Serie	*237*	*250*	*250*	*225*	*225*	*225*
1	0/0	90*/0	0/70	92/0	0/0	100/0
2	0/0	95*/0	0/100	98/0	75/0	100/0
3	90/0	100/0	0/70	100/0	100/0	100/0
4	100/0	85/0		100/0	100/0	
5	90/0	95/0		18/82	82/18	

These particles were observed to approach the spillway but were never actually seen moving over. It is very likely that the particles moved over the spillway since velocity of the water is directed towards the spillway at this position and since the particles did not move to the turbines nor remained in the reservoir.

Table 3 Percentage seeding particles penetrating the guiding device. The figures in italic denote flow rate (m³/s) to the spillway and the turbines, respectively.

	Session 1			Session 2		
Drop	1	2	3	1	2	4
/	*50*	*50*	*50*	*16*	*16*	*16*
Serie	*237*	*250*	*250*	*225*	*225*	*225*
1	0	0	0	0	0	2
2	0	0	0	10	2	0
3	0	0	0	95	15	0
4	0	5		18	78	
5	10	30		0	0	

A significant number of particles that moved along the guiding device crossed it through spaces between the wooden wall segments and continued towards the spillway on the downstream side of the barrier; see Table 3 and Fig. 8. Hence, although passing the guiding device the particles did not go towards the turbines. Most of the particles released between the guiding device and the northern shore did, however, go to the turbines indicating that once at this position there is no flow towards the guiding device; see Table 2; Session 1, series 3. Hence, the particles that moved towards the turbines in drop 5 series 1 & 2 in Session 2 probably ended up in the gap between the guiding device and the northern shore.

The velocity vector fields derived from the sampled images from series 4 of Session 2, are shown Figs 8 where the mean particle speeds in the different drops are 0.23 m/s, 0.26 m/s and 0.19 m/s, respectively. As can be seen in the vector plots, all seeding particles in the bulk flow move towards the guiding device in the direction of the turbines and then follow the device towards the spillway. However, close to the spillway, some of the seeding particles stray away from the guiding device, which is most obvious in drop 3; Fig. 8. There are also a couple of the particles that penetrate the device and move on the down-stream side of it.
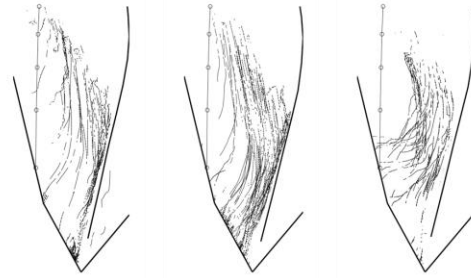

Fig. 8. Velocity fields as obtained with PTV from Session 2 series 4. The figures denote from left to right drops 1-3.

Stationary simulations are carried out with flow rates corresponding to series 2-3 in Session 1 (50 m3/s to the spillway and 250 m3/s to the turbines) and Session 2 (16 m3/s to the spillway and 225 m3/s to the turbines) and notice that the experimental conditions during series 1 in Session 1 are close to the ones for series 2-3 during the same session. The results show similar tendencies as the main part of the surface 2D streamlines indicates movement towards spillway B regardless of Session; see Fig. 9.
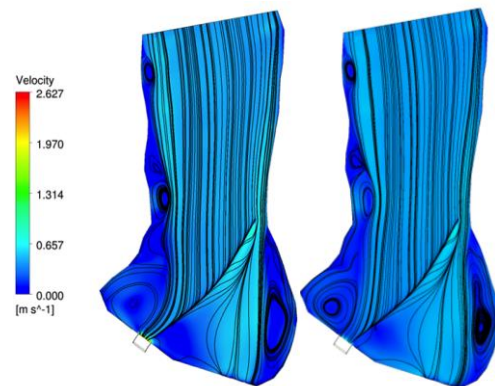

Fig. 9. Plot of surface velocity from CFD with 2D streamlines. Left: Conditions for drop 2-3 in Session 1. Right: Conditions for Session 2.

Three distinct routes are furthermore found if particles enter the space between the guiding device and the north shoreline. While the major part of the streamlines are directed towards the turbines some streamlines, depending on the location when entering the gap, follows either the guiding device towards spillway B or get caught in the swirling flow close to the shoreline. The swirls are even more prominent close to the south shoreline; see Fig. 9. There is a large circulation formed between the guiding device and the southern shoreline as also observed from debris motions during the field measurements. Up-stream this circulation there are two smaller circulations in which particles can be trapped if they come too close. Another observation is that the higher mass flow rate through the spillway in Session 1 implies a somewhat more condensed collection of streamlines in the main flow.

Streamlines originating from approximately 50 m upstream the dam are examined for comparison

with drop 4 in Session 2, see Fig. 10. The result show similar trends, as the majority of the surface flow is moving towards the spillway; cf Fig. 8 with Fig. 10. The streamlines furthermore show an average velocity of 0.26 m/s, which is to be compared to the average velocity between 0.19-0.26 m/s retrieved from the field experiments. The agreement between simulations and experiments is therefore very good.

With the simulations it is also possible to examine the formation of secondary flow close to the guiding device. A vector plot representing the velocity in Session 2 shows circulation of water on the northern side of the guiding device, see Fig. 11. The velocity vectors indicate that particle transport on the water surface close to the guiding device is directed towards the spillway rather than the turbines. This is in agreement with experimental results, see for instance the tracks of particles down-stream the guiding device in Fig. 8.

6. DISCUSSION AND CONCLUSIONS

The device studied guide nearly all passively flowing objects at the surface of the water (in this case oranges) towards the spillways. It is however clear that the efficiency of the device can increase even more. Particles passing too close to the northern shoreline (drop position 5, Fig. 2) can be drawn towards the turbines as verified by series 3 of study 1, series 1 of session 2 and the simulations. Prolonging the device in this direction would thus increase its efficiency. Also notice that objects located too close to the southern shoreline (drop position 1 and 2, see Fig. 2) can be caught in large-scale re-circulations, as verified by series 1 of session 1 and series 2 of session 2, and confirmed by the simulations.

In addition, the streamlines from the simulations close to the spillway compare well with the experimentally derived particle tracks at the same position and the velocities derived in the experiments are close to the averaged velocity as derived from the simulations. Taken together, the good agreement between the experimental and numerical results suggests that PTV is a promising technique that might be suitable for other river engineering problems as well, such as sediment transport (Souza, Schulz *et al.* 2010).
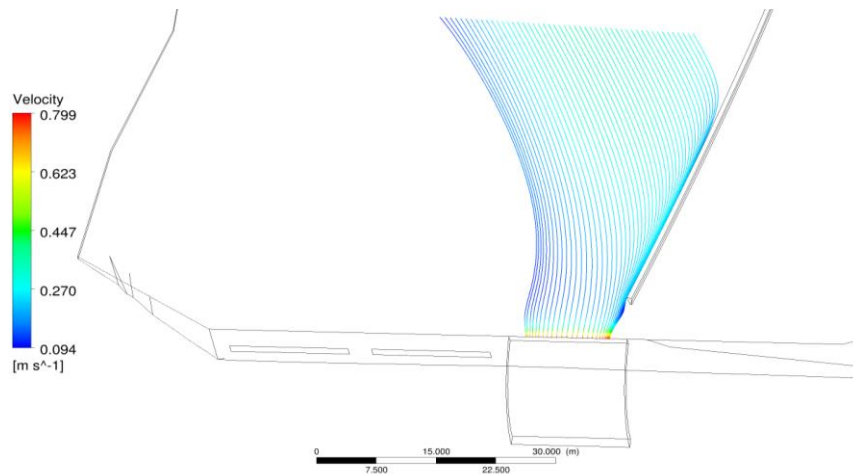

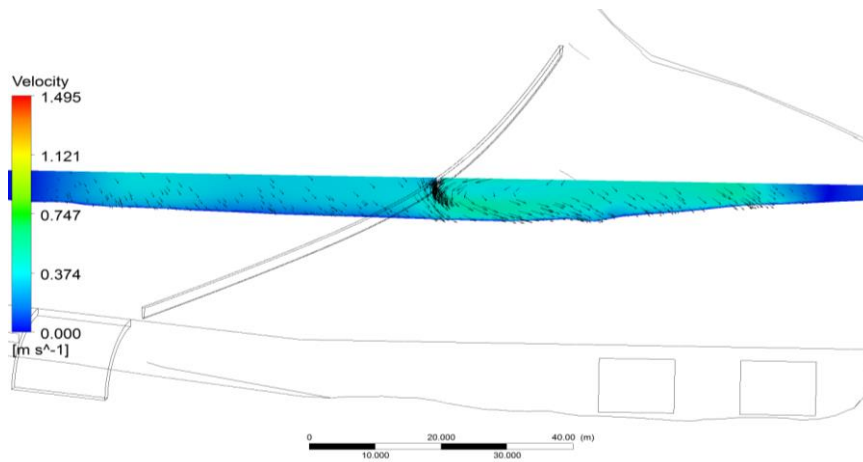**Fig. 10. Velocity and streamlines near the spillway.**

Fig. 11. Vector plot of velocity approximately 90 m upstream of the dam.

Another interesting result was that particles that passed through the guiding device, followed it on the downstream side; Figs 8. This shows the presence of secondary flow on the downstream side of the guiding device. A transport towards the spillways along the down-stream side of the guiding

device is also captured in the simulations; see Fig. 9. An easy way to improve further the efficiency of the guiding device is to extend it towards the northern shore of the river. Water flowing through the guiding device can most likely be stopped by creating a segment overlap. This can for example be accomplished by attaching a plate on the downstream side of each barrier segment or equipping each segment joint with a water tight rubber joint. Of course, the forces in the anchoring joints and the stresses in the guiding device will increase by such actions. It may on the other-hand be argued that the smolts will avoid moving between the segments and even if smolts would travel through the gaps both experiments and simulations show that flow in the close proximity of the downstream side of the guiding device will move towards spillway B rather than the turbines, implying that the relatively small gaps formed between the segments are of minor importance.

Although the experiments were carefully performed it must be pointed out that they were performed at a full-scale hydro power plant, implying in-field challenges generally absent in laboratory. Weather conditions are the largest difficulty with bright sun light, bursts of rain as well as baffling winds. Also, since some series lasted quite a long time, both clouds and sun moved during the samplings causing various shadows and reflections. To design a filter taking all this into account and successfully filters noise and background, leaving the seeding particles untouched is a considerable challenge.

Due to the great area covered by the water up-stream the dam, fenders and buoys were placed in the water. The main task of these objects was to serve as stationary points with known coordinates and distances. However, they were not perfectly stationary and moved slightly between the picture frames and the measurements. Even the fish guiding device displayed this movement, rendering the filtering process not only more difficult, but decreasing the accuracy and validity of the projective transformation. During the second study large secondary swirls were observed opposite to the guiding device close to the shore. Although these swirls never were captured in the photographs, it can be the reason for the large fraction of seeding particles deviating away from the guiding device close to the spillways during drop 4. Notice that at least one of these swirls was also captured in the simulations. To summarize, it has been demonstrated that:

● PTV is an appropriate technique in for the present case.

● PTV and CFD give similar results.

● The flow around the guiding device has a secondary swirl implying that the particles can move along the device on its down-stream side.

● Nearly all particles are guided to the spillway away from the turbines. This is a first step in the validation of the function of the fish guiding device. A second step would involve tagging of smolts.

● The relatively small spills imply that most of the water can be used for power production. It is also likely that if the guiding device can be shown to operate satisfactorily at these flow rates, it will also work for relatively higher flow rates over the spillways.

Future work could imply more detailed simulations with the aim to further optimize the shape of the guiding device and the detailed flow around it, for instance. Other issues are tagging of smolts and an evaluation of in-field Particle Tracking Velocimetry at alternative locations.

REFERENCES

Two-dimensional systems - SWEREF 99, projections. 2010. Lantmäteriet, SE-801 82 Gävle, Sweden.

normxcorr2; MATLAB - The Language Of Technical Computing. The MathWorks, Inc.; The MathWorks, Inc.

Abbasi, S. and N. Abbasi (2000). The likely adverse environmental impacts of renewable energy sources. *Applied energy* 65(1-4), 121-144.

Adrian, R. J.(1996). Laser Velocimetry. In: R.J. Goldstein (ed), Taylor & Francis, Washington, D.C.

Andersson, A. G., J. G. I. Hellström, P. Andreasson, and T. S. Lundström (2014). Effect of spatial resolution of rough surface on numerically computed flow field with application to hydraulic engineering. *Engineering Applications of Computational Fluid Mechanics* 8(3), 373–381.

Baek, S. J. and S. J. Lee (1996). A new two-frame particle tracking algorithm using match probability. *Experiments in Fluids* 22(1), 23-32.

Casey, M. and T. Wintergerste (2000). *ERCOFTAC Special Interest Group on Quality and Trust in Industrial CFD - Best Practice Guidelines Version 1.0*

Devernay, F. and O. Faugeras (2001). Straight lines have to be straight. *Machine Vision and Applications* 13(1), 14-24.

Fairchild, M. D. (2005). *Color appearance models.* J. Wiley.

Ferguson, J. W. (2005). The Behavior and Ecology of Downstream Migrating Atlantic Salmon (Salmo salar L.) and Brown Trout (Salmo trutta L.) in Regulated Rivers in Northern Sweden. *Vattenbruksinstitutionen, Rapport 44.*

Fujita, I., M. Muste, and A. Kruger (1998). Large-scale particle image velocimetry for flow analysis in hydraulic engineering applications. *Journal of Hydraulic Research* 36(3), 397-414.

Fujita, I. and M. Muste (2011). Preface to the special issue on image velocimetry. *Journal of Hydro-Environment Research* 5(4), 213.

Goldstein, R. J. and D. K. Kreid (1967). Measurement of laminar flow development in a square duct using a laser doppler flowmeter. *J. Appl. Mech* 34, 813-817.

Grabbe, M., K. Yuen, A. Goude, E. Lalander, and M. Leijon (2009). Design of an experimental setup for hydro-kinetic energy conversion. *International Journal on Hydropower and Dams* 16(5), 112-116.

Green, T. M., E. M. Lindmark, T. S. Lundström, and L.H. Gustavsson (2011). Flow characterization of an attraction channel as entrance to fishways. *River Research and Applications* 27(10), 1290-1297.

Haro, A., M. Odeh, J. Noreika, and T. Castro-Santos (1998). Effect of water acceleration on downstream migratory behavior and passage of Atlantic salmon smolts and juvenile American shad at surface bypasses. *Transactions of the American Fisheries Society* 127(1), 118-127.

Hassan, Y. A. and R. E. Canaan (1991). Full-field bubbly flow velocity measurements using a multiframe particle tracking technique. *Experiments in Fluids* 12(1), 49-60.

Hellström, J. G. I., B. D. Marjavaara, and T.S. Lundström (2007). Parallel CFD simulations of an original and redesigned hydraulic turbine draft tube. *Advances in Engineering Software* 38(5), 338-344.

Jodeau, M., A. Hauet, A. Paquier, J. Le Coz, and G. Dramais (2008). Application and evaluation of LS-PIV technique for the monitoring of river surface velocities in high flow conditions. *Flow Measurement and Instrumentatio,* 19(2), 117-127.

Johnson, G., N. Adams, R. Johnson, D. Rondorf, D. Dauble, and T. Barila (2000). Evaluation of the prototype surface bypass for salmonid smolts in spring 1996 and 1997 at Lower Granite Dam on the Snake River, Washington. *Transactions of the American Fisheries Society* 129(2), 381-397.

Kemp, P., M. Gessel, B. Sandford, and J. Williams (2005). Fine-scale behavioral responses of Pacific salmonid smolts as they encounter divergence and acceleration of flow. *Transactions of the American Fisheries Society* 134(2), 390-398.

Kemp, P., M. Gessel, B. Sandford, and J. Williams (2006). The behaviour of Pacific salmonid smolts during passage over two experimental weirs under light and dark conditions. *River Research and Applications* 22(4), 429-440.

Kusre, B. C., D. C. Baruah, P. K. Bordoloi, and S. C. Patra (2010). Assessment of hydropower potential using GIS and hydrological modeling technique in Kopili River basin in Assam (India). *Applied Energy* 87(1), 298-309.

Laine, A., R. Kamula, and J. Hooli (1998). Fish and lamprey passage in a combined Denil and vertical slot fishway. *Fisheries Management and Ecology* 5, 31-44.

Laine, A., T. Ylinäaräa, J. Heikkiläa, and J. Hooli (1998). *Behaviour of upstream migrating Whitefish, Coregonus lavaretus in the Kukkolankoski rapids*. Northern Finland: M. Jungwirth, S. Schmutz and S. Weiss, eds. In: *Fish Migration and Fish Bypasses* 1998, Fishing News Books, 33-44.

Lalander, E. and M. Leijon (2011). In-stream energy converters in a river - Effects on upstream hydropower station. *Renewable Energy* 36(1), 399-404.

Larsson, I. A. S., E. M. Lindmark, T. S. Lundström, D. Marjavaara, and S. T\OYRÄ (2012). Visualization of Merging Flow by Usage of PIV and CFD with Application to Grate-Kiln Induration Machines. *Journal of Applied Fluid Mechanics* 6.

Lindmark, E. and L. H. Gustavsson (2008). Field study of an attraction channel as entrance to fishways. *River Research and Applications* 24(5), 564-570.

Ljung, A. L., T. S. Lundström, B. Daniel Marjavaara, and K. TANO (2011). Convective drying of an individual iron ore pellet - Analysis with CFD. *International Journal of Heat and Mass Transfer* 54(17-18), 3882-3890.

Lundström, T. S., J. G. I. Hellström, and E.M. Lindmark (2010). Flow design of guiding device for downstream fish migration. *River Research and Applications* 26(2), 166-182.

Marjavaara, B. D. and T. S. Lundström (2006). Redesign of a sharp heel draft tube by a validated CFD-optimization. *International Journal for Numerical Methods in Fluids* 50(8), 911-924.

Marjavaara, B. D. and T. S. Lundström, T. Goel, Y. Mack, and W. Shyy (2007). Hydraulic turbine diffuser shape optimization by multiple surrogate model approximations of Pareto fronts. *Journal of Fluids Engineering, Transactions of the ASME* 129(9), 1228-1240.

Meselhe, E., T. Peeva, and M. Muste (2004). Large scale particle image velocimetry for low velocity and shallow water flows. *Journal of Hydraulic Engineering-Asce* 130(9), 937-940.

Moore, A., S. Ives, T. Mead, and L. Talks (1998). The migratory behaviour of wild Atlantic salmon (Salmo salar L.) smelts in the River Test and Southampton Water, southern England. *Hydrobiologia,* 372, 295-304.

Pompeu, P. S., A. A. Agostinho, and F. M. Pelicice (2012). Existing and future challenges: the concept of successful fish passage in south america. *River Research and Applications,* 28(4), 504-512.

Price, T. and D. Probert (1997). Harnessing hydropower: A practical guide. *Applied Energy* 57(2-3), 175-251.

Renöfält, B. M., R. Jansson, and C. Nilsson (2010). Effects of hydropower generation and opportunities for environmental flow management in Swedish riverine ecosystems. *Freshwater Biology* 55(1), 49-67.

Rice, S. P., J. Lancaster, and P. Kemp (2010). Experimentation at the interface of fluvial geomorphology, stream ecology and hydraulic engineering and the development of an effective, interdisciplinary river science. *Earth Surface Processes and Landforms* 35, 64-77.

Roache, P. J. (1997). Quantification of uncertainty in computational fluid dynamics. *Annual Review of Fluid Mechanics* 29, 123-160

Rodrigueaz, J. F., F. A. Bombbardelli, M.H. García, K.M. Frothingham, B.L. Rhoads, and J.D. Abad (2004). High-resolution numerical simulation of flow through a highly sinuous river reach. *Water Resources Management* 18(3), 177-199.

Rowland, E., R. Hotchkiss, and M. Barber (2003). Predicting fish passage design flows at ungaged streams in eastern Washington. *Journal of Hydrology* 273(1-4), 177-187.

Ruggles, C. P., D. A. Robinson, and R. J. Stira (1993). The use of floating louvers for guiding Atlantic salmon smolts from hydroelectric turbine intakes. *Can.Tech.Rep.Fish.Aquat.Sci.,* 1905, 87-94.

Ruggles, C.P. and P. Ryan (1964). An investigation of louvers as a method of guiding juvenile Pacific salmon. *Canadian Fish Culturist,* 33, 3-67.

Russell, I., A. Moore, S. Ives, L. Kell, M. Ives, and R. Stonehewer (1998). The migratory behaviour of juvenile and adult salmonids in relation to an estuarine barrage. *Hydrobiologia* 372, 321-333.

Schilt, C. R. (2007). Developing fish passage and protection at hydropower dams. *Applied Animal Behaviour Science,* 104(3-4), 295.

Scruton, D., L. Ollerhead, K. Clarke, C. Pennell, K. Alfredsen, A. Harby, and D. Kelly (2003). The behavioural response of juvenile Atlantic salmon (Salmo salar) and brook trout (Salvelinus fontinalis) to experimental hydropeaking on a newfoundland (Canada) River. *River Research and Applications* 19(5-6), 577-587.

Souza, L. B. S., H. E. Schulz, S. M. Villela, and J. S. Gulliver, (2010). Experimental Study and Numerical Simulation of Sediment Transport in a Shallow Reservoir. *Journal of Applied Fluid Mechanics* 3(2), 9-21.

Taft, E. P. (2000). Fish protection technologies: A status report. *Environmental Science and Policy,* 3(SUPPL. 1), 349-359.

Tarkowski, R. and B. Uliasz-Misiak (2003). Renewable energy sources in Guadeloupe. *Applied Energy* 74(1-2), 221-228.

Vashisht, A. K. (2012). Current status of the traditional watermills of the Himalayan region and the need of technical improvements for increasing their energy efficiency. *Applied Energy* 98, 307-315.

Whitney, R. R., L. D. Calvin, M. W. Erho, and C. C. Coutant (1997, October). *Downstream Passage for Salmon at Hydroelectric Projects in the Columbia River Basin: Development, Installation, And Evaluation.* Published October 1997 by the Northwest Power Planning Council.

Wintergerste, T., M. Casey, and A. G. Hutton (2002). The best practice guidelines for CFD - A European initiative on quality and trust, *American Society of Mechanical Engineers, Pressure Vessels and Piping Division (Publication) PVP* 2002, 1-10.